ACS SENSORS

pubs.acs.org/acssensors Article

Highly Efficient PTCA/Co_3O_4/CuO/$S_2O_8^{2-}$ Ternary Electrochemiluminescence System Combined with a Portable Chip for Bioanalysis

Xianzhen Song, Lu Zhao, Xiang Ren, Tao Feng, Hongmin Ma, Dan Wu, Yuyang Li,* Chuannan Luo, and Qin Wei

Cite This: *ACS Sens.* 2022, 7, 2273−2280 Read Online

ACCESS | Metrics & More | Article Recommendations | Supporting Information

ABSTRACT: Herein, we reported an efficient electrochemiluminescence (ECL) biosensor chip for sensitive detection of neuron-specific enolase (NSE). First, 3,4,9,10-perylenetetracarboxylic acid with good luminescence characteristics was used as a luminophore to obtain a stable ECL signal. Subsequently, hollow porous Co_3O_4/CuO concave polyhedron nanocages (CPNCs) were designed as co-reaction promoters to amplify the luminescence signals for highly sensitive trace detection of NSE. In brief, the rapid cyclic conversion of Co^{3+}/Co^{2+} and Cu^{2+}/Cu^{+} redox pairs could continuously catalyze the reduction of persulfate ($S_2O_8^{2-}$), thus providing a large number of essential active intermediates ($SO_4^{\bullet-}$) for ECL emission. Meanwhile, the unique structure of Co_3O_4/CuO CPNCs possessed a large specific surface area, which greatly improved its catalytic efficiency. Third, NKFRGKYKC was developed as an affinity ligand for specific antibody fixation, which improved incubation efficiency and protected bioactivity of antibodies. Finally, we independently designed a microchip and applied it for ECL detection to improve the practical application ability of the sensor. The developed biosensor exhibited good sensitivity with a wide linear range (10 fg/mL to 100 ng/mL) and a low detection limit (3.42 fg/mL), which played an active role in the clinical application of sensing analysis.

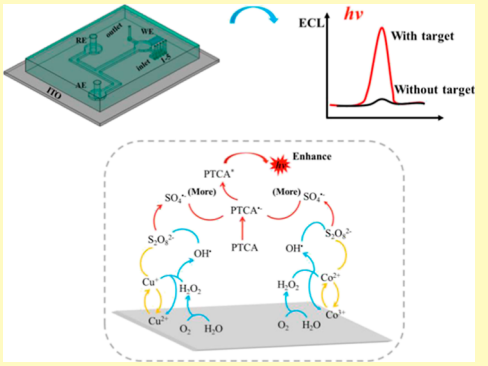

KEYWORDS: *electrochemiluminescence, biosensor chip, Co_3O_4/CuO CPNCs, co-reaction promoter, NKFRGKYKC*

Electrochemiluminescence (ECL) is specific chemiluminescence initiated by electrochemistry, which retains the good peculiarities of chemiluminescence, for instance, high sensitivity and a wide response range.[1,2] Meanwhile, it also has the advantages of stable luminescence signals, strong temporal and spatial controllability, and high reproducibility.[3,4] For the moment, ECL has been used in immunoassay,[5,6] environmental monitoring,[7,8] cell analysis,[9,10] and other fields.

Neuron-specific enolase (NSE) is a specific acidic protease of neurons and neuroendocrine cells.[11] As a macromolecular protein, its molecular weight is 78 kD.[12] NSE is overexpressed in small-cell lung cancer (SCLC), resulting in significantly elevated serum NSE (the normal value is less than 15 ng/mL).[13,14] Therefore, NSE is one of the preferred markers for SCLC clinical diagnosis. In addition, because the serum NSE level in SCLC is higher than that in non-small-cell lung cancer (NSCLC), it is also used for the differential diagnosis of SCLC and NSCLC.[15] Herein, we developed an ECL biosensor for NSE trace detection.

As an organic perylene dye, 3,4,9,10-perylenetetracarboxylic acid (PTCA) has high application prospects in the field of electrochemistry because of large specific surface areas and excellent conductivity and film-forming properties.[16−18] Meanwhile, PTCA also exhibits excellent organic electronic and optical properties,[19,20] which has stable ECL emissions in persulfate ($S_2O_8^{2-}$), so we selected it as an ideal luminophore. To increase sensitivity of the biosensor, a ternary ECL system was designed to amplify ECL signals. Herein, we developed hollow porous Co_3O_4/CuO concave polyhedral nanocage (CPNC) heterojunctions as co-reaction promoters by using metal−organic frameworks (MOFs) as self-sacrificing templates.[21] The prepared Co_3O_4/CuO CPNCs showed high catalytic efficiency for the decomposition of $S_2O_8^{2-}$ because of its large specific surface area and variable valence states of metal ions.

The sensitivity and stability of the biosensor are affected by antigen binding capacity, and the antigen binding sites are distributed in the variable regions (Fab fragments) of the antibodies.[22,23] The traditional antibody fixation methods are random, which cannot avoid an occupation of Fab fragments,

Received: April 15, 2022
Accepted: July 19, 2022
Published: August 3, 2022

Scheme 1. Fabrication Process of the Biosensor

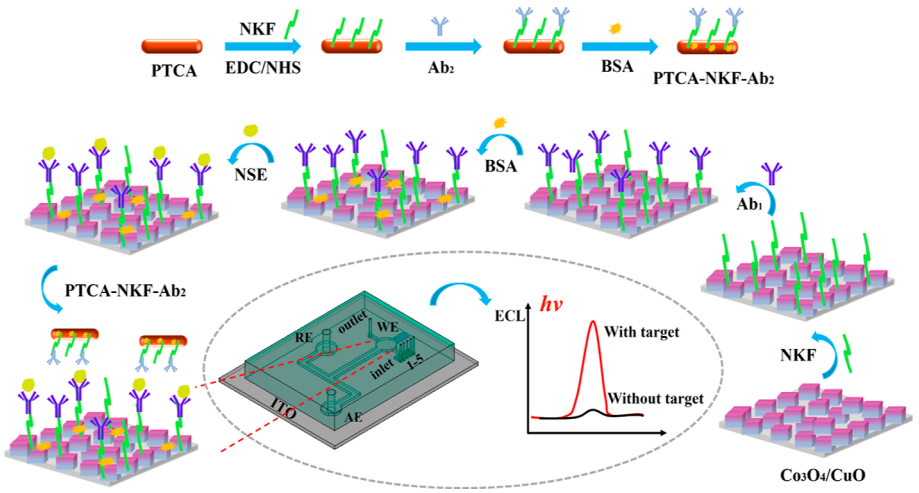

thus affecting antigen binding ability of the antibodies.[24] NKFRGKYKC (NKF), as a short peptide ligand, specifically links Fc fragments of antibodies to protect its antigen binding activity.[25] Therefore, antibodies immobilized based on NKF could recognize and capture antigens more quickly and effectively, thus improving biosensor sensitivity. In addition, due to the protection of antibody activity by NKF, the storage time of the sensor was prolonged, thereby improving its stability. Combined with the related references and experimental results,[26−28] we inferred that NKF improved the sensitivity and storage stability of the biosensor through a targeted antibody immobilization strategy.

In this work, we developed an efficient ECL biosensor for NSE trace detection. First, PTCA was selected as a luminophore to gain stable ECL emission. Second, Co_3O_4/CuO CPNCs with high catalytic ability were prepared to promote the reduction of $S_2O_8^{2-}$ for more sulfate radicals ($SO_4^{\bullet-}$), so as to obtain a strong luminescence signal. Specifically, the two redox pairs of Cu^+/Cu^{2+} and Co^{3+}/Co^{4+} in it could continuously react with $S_2O_8^{2-}$ through the reversible conversion of the valence state, thereby generating a large amount of $SO_4^{\bullet-}$. At the same time, its unique hollow structure showed a large specific surface area, which further improved the catalytic efficiency. Third, NKF was introduced for the directional fixation of antibodies, which protected the activity and improved the sensitivity of the biosensor. Finally, we designed a portable detection chip based on a three-electrode system to improve the practical application ability of the biosensor, which exhibited many unique advantages. In brief, the ECL sensor based on the chip possessed the peculiarities of miniaturization and less reagent consumption. Subsequently, the portability of the chip can realize the real-time detection of samples, thus improving practical application ability and detection efficiency of the sensor. Furthermore, all ECL reactions are carried out in the chip, which reduces the pollution of the samples and improves storage stability of the sensor. The developed biosensor showed a low detection limit (3.42 fg/mL), providing a positive reference for the clinical real-time diagnosis of sensing analysis.

EXPERIMENTAL SECTION

Reagents and Apparatus. NSE, NSE primary (Ab_1) and secondary (Ab_2) antibodies, and NKFRGKYKC were acquired from Nanjing Kingsrui Technology Co., Ltd. Cobalt nitrate hexahydrate [$Co(NO_3)_2{\cdot}6H_2O$], copper nitrate hexahydrate [$Ce(NO_3)_2{\cdot}6H_2O$], ferric chloride ($FeCl_3$), and bovine serum albumin (BSA, 96%) were gained from Macklin Biochemical Co., Ltd. All reagents used in the system were of analytical grade, and ultrapure water (18.25 MΩ·cm^{-1}) was used throughout the work.

X-ray powder diffraction (XRD) patterns were obtained with a D8 ADVANCE X-ray diffractometer (Bruker AXS, Germany). The microstructure of nanomaterials was characterized by scanning electron microscopy (SEM, JEOL JSM-6700F, Japan) and transmission electron microscopy (TEM, JEOL JEM-2100F, Japan). The elemental composition of the synthesized nanomaterials was obtained by X-ray photoelectron spectroscopy (XPS, ESCALAB MK II, UK). Fluorescence (FL) emission spectra were acquired under excitation at 365 nm using an Edinburgh Instruments FLS920 spectrometer (Edinburgh Instruments, UK). The ECL signal was detected using an MPI-E electrochemiluminescence analyzer (Xi'an remax Electronic Science Tech. Co., Ltd).

Preparation of PTCA-NKF-Ab_2 Signal Probes. First, 50 mg of 3,4,9,10-perylenetetracarboxylic dianhydride was dissolved in 25 mL of NaOH solution and heated to complete dissolution. Subsequently, the dilute HCl (1 M) was added until its color changed from yellow green to red, thereby obtaining PTCA. Next, the prepared PTCA was dispersed in 5 mL of phosphate-buffered saline (PBS), and then, a 2 mL mixture of EDC (40 mM) and NHS (10 mM) was added to activate its carboxyl groups. After that, 1 mL of NKF was dispersed in it to obtain PTCA-NKF through the aldol condensation reaction. Finally, 100 μL of Ab_2 and 8 μL of BSA (1%) were added successively to acquire PTCA-NKF-Ab_2 signal probes.

Preparation of Co_3O_4/CuO CPNCs. Co_3O_4/CuO CPNCs were synthesized according to previous reports with minor modifications.[21] Briefly, 0.66 g of 2-methylimidazole and 0.5 g of $Co(NO_3)_2{\cdot}6H_2O$ were successively dissolved in 50 mL of methanol named solution 1 (S1) and solution 2 (S2), respectively. Afterward, S1 was slowly poured into S2 and stirred evenly. After standing for 24 h, the ZIF-67 template was obtained by centrifugation and washing. Next, 150 mg of ZIF-67 template was dissolved in 100 mL of ethanol, and then, 25 mg of $Cu(NO_3)_2{\cdot}6H_2O$ was added. Finally, the precipitate was collected by centrifugation, washing, and drying and then calcined at 500 °C for 2 h to obtain Co_3O_4/CuO CPNCs.

Subsequently, the prepared Co_3O_4/CuO was aminated. Specifically, 50 mg of Co_3O_4/CuO was dissolved in the mixture of 30 mL of ethanol and 2 mL of ultrapure water. Afterward, 2 mL of $NH_3{\cdot}H_2O$ and 200 μL of (3-aminopropyl)trimethoxysilane were added with ultrasound for 10 h. Finally, the functionalized Co_3O_4/CuO was acquired by centrifugation and washing.

Preparation of the Chip. First, the electrode substrate needed to be prepared. Specifically, the ink was printed on the treated indium tin oxide (ITO) with a self-made screen printing template and then dried

https://doi.org/10.1021/acssensors.2c00819
ACS Sens. 2022, 7, 2273−2280

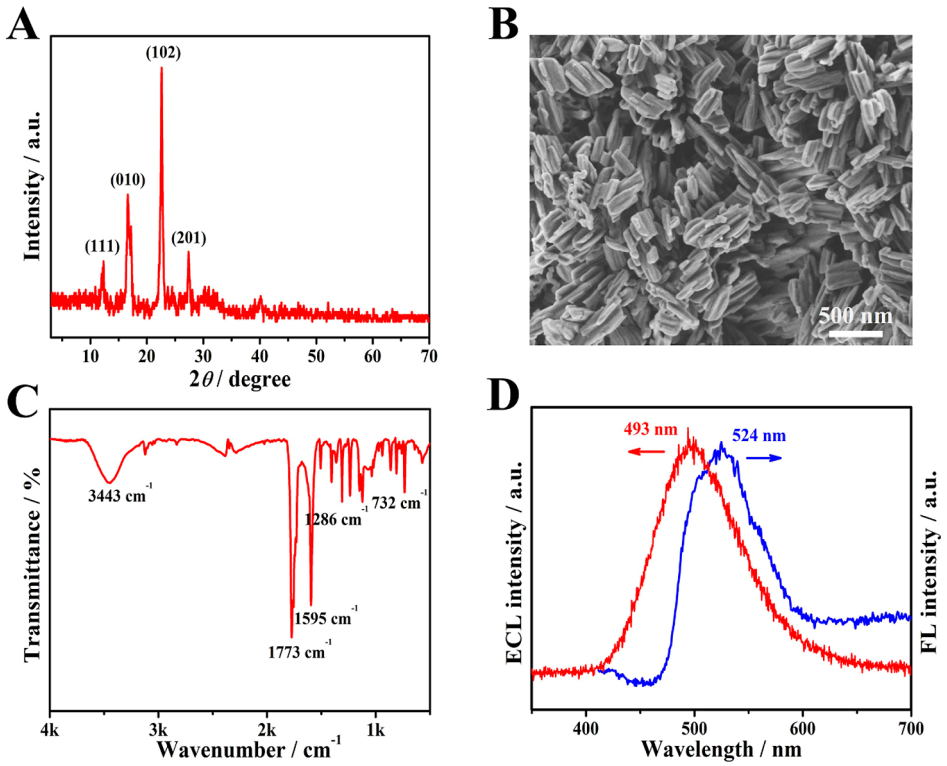

Figure 1. Characterization of PTCA. (A) XRD pattern, (B) SEM image, and (C) FT-IR spectrum of PTCA. (D) ECL (red curve) and FL spectra (blue curve) of PTCA.

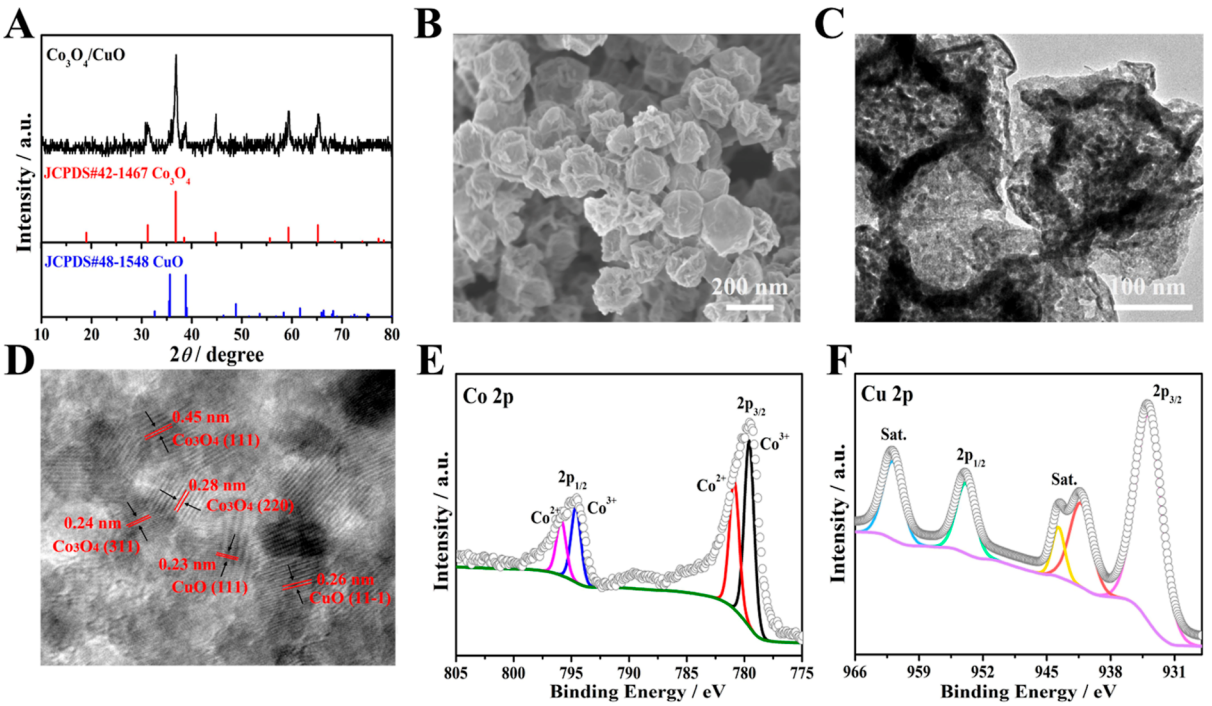

Figure 2. Characterization of Co_3O_4/CuO. (A) XRD pattern, (B) SEM, (C) TEM, and (D) HRTEM images of Co_3O_4/CuO. XPS spectra of (E) Co 2p and (F) Cu 2p regions of Co_3O_4/CuO.

at 120 °C. Afterward, the conductivity of ITO was removed by wet etching (etching solution: $FeCl_3$/HNO_3/HCl = 0.5 M/1 M/1 M), and then, the ink was washed with acetone. Next, the processed ITO was sonicated in ethanol and boiled in KOH solution. Finally, the functionalized Co_3O_4/CuO was modified on it as an initial working electrode to obtain the electrode substrate.

Subsequently, a polydimethylsiloxane microchannel was fabricated by soft lithography, and the microchannel and the electrode substrate were surface-treated with oxygen plasma for 50 s to bond them. Afterward, the prepared chip was heated to bond it firmly. Next, the reference electrode (Ag/AgCl) and the auxiliary electrode (Pt electrode) were inserted into the chip through the reserved electrode hole. Thus, the chip integrating the three-electrode detection system

https://doi.org/10.1021/acssensors.2c00819
ACS Sens. 2022, 7, 2273−2280

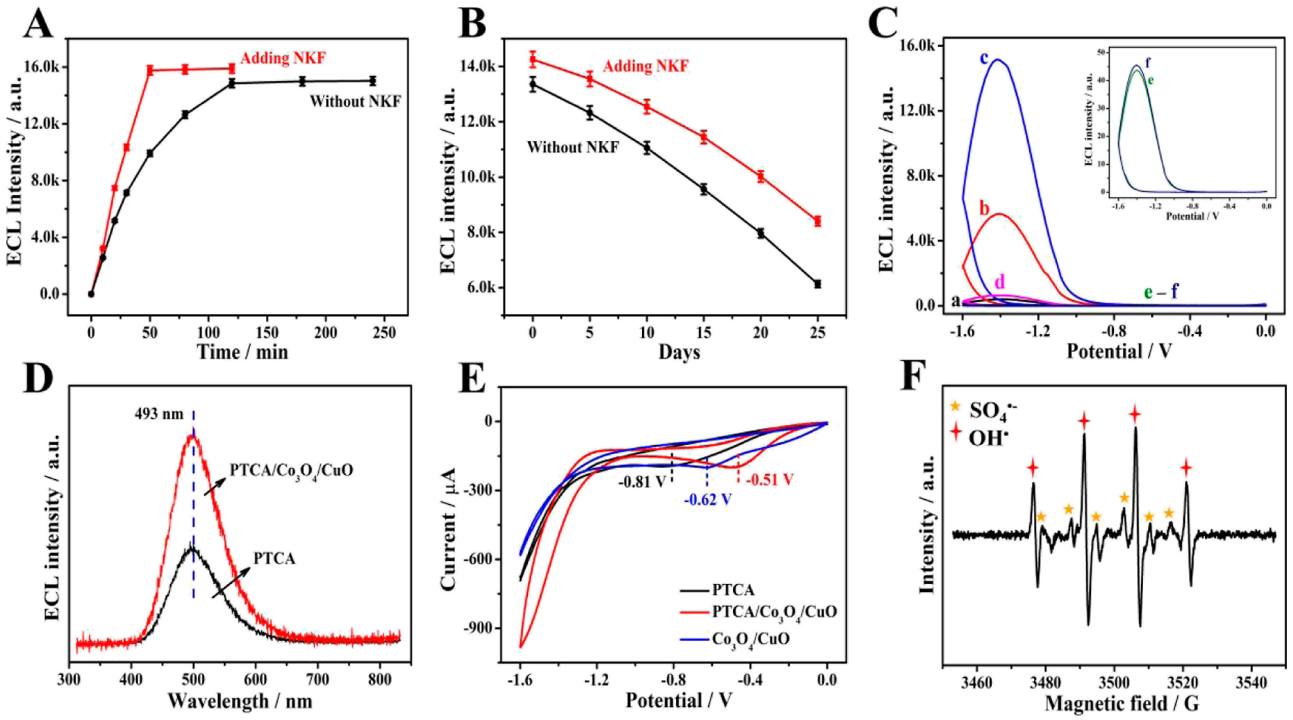

Figure 3. ECL, CV, and EPR tests of the reaction system. (A) ECL signals of the biosensors at different antibody incubation times. (B) ECL signals of the biosensors after different storage times. (C) ECL responses of (a) bare electrode, (b) PTCA, (c) PTCA/Co_3O_4/CuO, and (d) Co_3O_4/CuO in 50 mM $S_2O_8^{2-}$ and (e) PTCA and (f) PTCA/Co_3O_4/CuO in PBS. (D) ECL spectra of PTCA and PTCA/Co_3O_4/CuO in 50 mM $S_2O_8^{2-}$. (E) CV curves of PTCA, PTCA/Co_3O_4/CuO, and Co_3O_4/CuO in 50 mM $S_2O_8^{2-}$. (F) EPR spectrum analysis.

has been successfully prepared. The diagram of the preparation of the chip is presented in the Supporting Information.

Fabrication of the Biosensor. The specific fabrication process is shown in Scheme 1. First, 10 μL of the carboxyl-activated NKF was injected into the chip through inlet 1 to connect the substrate materials. After that, 20 μL of Ab_1 and 5 μL of BSA were injected successively through inlets 2 and 3 and then incubated for 2 h. Next, 15 μL of different concentrations of NSE was introduced through inlet 4 and incubated for 50 min. Finally, the prepared PTCA-NKF-Ab_2 probes (20 μL) were injected through inlet 5, and thus, the biosensor was successfully fabricated. During the construction process of the biosensor, PBS was introduced for washing to remove the unbound reagents. The injection flow rate for all samples was 5 μL/min.

Measurement Conditions. ECL testing was implemented through a self-assembled chip integrating a three-electrode system. $K_2S_2O_8$ solution was injected into the chip as coreactants. The detection apparatus was a MPI-F flow injection chemiluminescence detector, the photomultiplier tube voltage was 600 V, and the scanning voltage range was −1.6 to 0 V.

RESULTS AND DISCUSSION

Characterization of PTCA. In Figure 1A, the XRD pattern of PTCA shows four diffraction peaks, which are assigned to the (111), (010), (102), and (201) crystal planes.[16,29] The SEM image of PTCA (Figure 1B) revealed a short rod-like structure (450 nm). In Figure 1C, the Fourier transform infrared (FT-IR) spectrum of PTCA shows several characteristic peaks. Specifically, the three peaks at 3443, 1773, and 1286 cm^{-1} corresponded to ν_{O-H}, $\nu_{C=O}$, and ν_{C-O}, suggesting the presence of carboxyl groups. Meanwhile, the other peaks at 1595 and 733 cm^{-1} were attributed to $\nu_{C=C}$ and $\delta_{=C-H}$, which indicated the existence of aromatic rings.[19,30] Figure 1D shows the FL and ECL emission spectra of PTCA, and an obvious ECL emission peak appeared at 493 nm. Meanwhile, the FL emission peak position of PTCA was 524 nm under an excitation light source of 365 nm. These results demonstrated the successful preparation of PTCA, and the prepared PTCA had good luminescence properties.

Characterization of Co_3O_4/CuO CPNCs. According to the XRD patterns (Figure 2A), the characteristic peaks of Co_3O_4/CuO were indexed as the cubic phase of Co_3O_4 (JCPDS 42-1467) and the monoclinic phase of CuO (JCPDS 48-1548). Meanwhile, no other diffraction peaks were observed, confirming the coexistence of the two metal oxides. In Figure 2B, the SEM image of Co_3O_4/CuO shows a concave polyhedron structure with a uniform particle size (200 nm). The TEM image displayed that Co_3O_4/CuO was composed of multiple small nanoparticles and possessed a hollow porous structure (Figure 2C). In addition, lattice fringes were observed in the high-resolution transmission electron microscopy (HRTEM) image. Specifically, a fringe spacing of 0.45, 0.28, and 0.24 nm was attributed to (111), (220), and (311) crystal planes of Co_3O_4, respectively. At the same time, a fringe spacing of 0.23 and 0.26 nm was attributed to (111) and (11-1) crystal planes of CuO, respectively (Figure 2D). The elemental composition and valence state of Co_3O_4/CuO were studied by XPS. In Figure S2A, we observed all elements of Cu, Co, and O in Co_3O_4/CuO. In Figure 2E, the two characteristic peaks at 796.2 and 794.6 eV ar attributed to Co^{2+} $2p_{1/2}$ and Co^{3+} $2p_{1/2}$, while the peaks at 781.2 and 779.4 eV belong to Co^{2+} $2p_{3/2}$ and Co^{3+} $2p_{3/2}$.[31−33] The Cu 2p spectrum of Co_3O_4/CuO (Figure 2F) showed a Cu $2p_{1/2}$ peak at 953.6 eV and a satellite peak at 962.3 eV. Meanwhile, the characteristic peak at 934.2 eV belonged to Cu $2p_{3/2}$, and the corresponding satellite peaks were observed at 941.3 and 943.6 eV.[34,35] According to the XPS spectrum of the O 1s region (Figure S2B), the peak at 529.5 eV could be attributed to the

https://doi.org/10.1021/acssensors.2c00819
ACS Sens. 2022, 7, 2273−2280

metal−oxygen bonds (O^{2-}),[31,34] and the peak of 531.2 eV may belong to OH^- of defective oxide and hydroxyl groups.[36,37]

Effects of NKF in the Biosensor. To explore the function of the affinity ligands on antibody incubation efficiency, the ECL responses of the constructed biosensors after different antibody incubation times were studied. As shown in Figure 3A, the ECL responses of the proposed sensor were continuously enhanced with an increase in antibody incubation time and then tended to be stable at 50 min (red curve). In addition, the ECL signals of the control sensor without NKF leveled off after 120 min, and the final ECL response was also lower than that of the proposed sensor (black curve). Therefore, the results indicated that NKF improved the antibody incubation efficiency.

Subsequently, we tested the signal attenuation degree of the developed biosensor stored for different times. In Figure 3B, the ECL signals gradually decreased with an extension of the storage time. When the storage time reached 25 days, the ECL response of the biosensor-introduced NKF decreased to 8406 a.u. (red curve). After calculation, the corresponding signal attenuation rate was 41%, while that of the sensor without NKF was 54% (black curve). The above results showed that NKF protected the activity of the biosensor, thereby prolonging its storage time.

Signal Amplification Mechanism. First, the ECL signals of different modified electrodes were detected in PBS containing 50 mM $S_2O_8^{2-}$. As shown in Figure 3C, the bare electrodes showed a little ECL emission response. After PTCA was modified on the electrode, it exhibited an obvious ECL response, which was attributed to the reaction between PTCA and $S_2O_8^{2-}$. After continuous modification with Co_3O_4/CuO, PTCA/Co_3O_4/CuO showed a strong ECL signal, which was about 2.7 times than that of PTCA. The results illustrated that the introduction of Co_3O_4/CuO greatly improved the above reaction. Meanwhile, Co_3O_4/CuO exhibited a stronger ECL signal than that of the bare electrodes, suggesting that it could interact with $S_2O_8^{2-}$ to enhance the ECL response. In addition, we also tested the ECL responses of PTCA and PTCA/Co_3O_4/CuO in pure PBS, and the results showed that none of them produced ECL emission. Subsequently, the ECL spectra of PTCA and PTCA/Co_3O_4/CuO were obtained to further investigate the signal amplification mechanism. In Figure 3D, the ECL intensity of PTCA/Co_3O_4/CuO was increased compared to that of PTCA. Meanwhile, the corresponding peak position did not change (493 nm). Thus, we concluded that Co_3O_4/CuO did not react with PTCA.

In addition, the CV curves of PTCA, PTCA/Co_3O_4/CuO, and Co_3O_4/CuO were also investigated. In Figure 3E, the reduction peak potential of PTCA/Co_3O_4/CuO-modified electrode shifted positively (−0.81 to −0.51 V) compared to that of PTCA. Co_3O_4/CuO promoted the reduction of $S_2O_8^{2-}$, thereby accelerating the reaction of PTCA and $S_2O_8^{2-}$. Therefore, the lowering of the reaction barrier reduced $S_2O_8^{2-}$ at a weaker negative potential (absolute value). Meanwhile, the peak current increased accordingly, which was due to the reduction of the reaction barrier that sped up the reaction rate, thereby promoting the electron transfer process in the solution. Furthermore, the CV response of pure Co_3O_4/CuO in $S_2O_8^{2-}$ was also explored, and the measured reduction potential was 0.62 V, which further confirmed the promoting effect of Co_3O_4/CuO on the reduction of $S_2O_8^{2-}$. However, the reduction of $S_2O_8^{2-}$ was slightly inhibited due to the lack of luminophores that reacted with the reduced product. Therefore, the positive shift degree of reduction potential of the Co_3O_4/CuO-modified electrode is weaker than that of PTCA/Co_3O_4/CuO. These results strongly confirmed that Co_3O_4/CuO could not act on PTCA but indirectly improved luminescence signals by promoting the reduction of $S_2O_8^{2-}$.

To visually verify the proposed reaction mechanisms, we measured the free radicals in this system by in situ electron paramagnetic resonance (EPR) spectroscopy. Herein, the EPR spectrum of the PTCA/Co_3O_4/CuO/$S_2O_8^{2-}$ system was tested by using 5,5-dimethyl-1-pyrroline *N*-oxide (DMPO) as a free radical trapping agent. As shown in Figure 3F, we observed a typical quadruple peak with the peak intensity ratio of 1:2:2:1, corresponding to the DMPO-OH adducts, which verified the generation of hydroxyl radicals ($OH^\bullet$).[38−40] At the same time, there were two small peaks between the above four characteristic peaks, which was the characteristic of DMPO-SO_4 adducts, indicating the presence of $SO_4^{\bullet-}$.[17,41] In conclusion, we could confirm that $OH^\bullet$ and $SO_4^{\bullet-}$ were generated in the system, confirming the proposed reaction mechanisms.

Possible ECL Mechanism. The possible luminescence mechanism is shown in Figure 4. First, $S_2O_8^{2-}$ could obtain

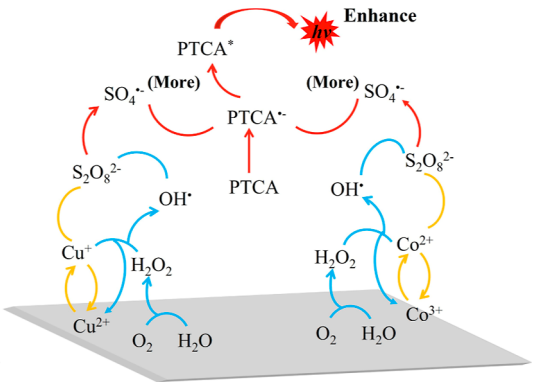

Figure 4. Schematic diagram of the ECL mechanism.

electrons to produce less $SO_4^{\bullet-}$ (route 1). After that, Co^{3+}/Co^{2+} and Cu^{2+}/Cu^+ redox couples accelerated the generation of $SO_4^{\bullet-}$. Briefly, Co^{3+}/Co^{2+} could capture electrons to produce Co^{2+}/Cu^+ and then reacted with $S_2O_8^{2-}$ to obtain a large amount of $SO_4^{\bullet-}$ (orange lines, route 2). Furthermore, $OH^\bullet$ was generated through a series of redox reactions, and then, the obtained $OH^\bullet$ further reacted with $S_2O_8^{2-}$ to generate more $SO_4^{\bullet-}$ (blue lines, route 3). For the ECL emission process, PTCA first gained electrons to produce $PTCA^{\bullet-}$ and then reacted with $SO_4^{\bullet-}$ to generate PTCA*. Finally, the obtained PTCA* transitioned back to the ground state and produced ECL emission (red lines). The reaction mechanism formulas were as follows.

Route 1:

$$S_2O_8^{2-} + e^- \rightarrow SO_4^{2-} + SO_4^{\bullet-} \quad (1)$$

Route 2:

$$Co^{3+}/Cu^{2+} + e^- \rightarrow Co^{2+}/Cu^+ \quad (2)$$

$$Co^{2+}/Cu^+ + S_2O_8^{2-} \rightarrow Co^{3+}/Cu^{2+} + SO_4^{2-} + SO_4^{\bullet-}(\text{more}) \quad (3)$$

https://doi.org/10.1021/acssensors.2c00819
ACS Sens. 2022, 7, 2273−2280

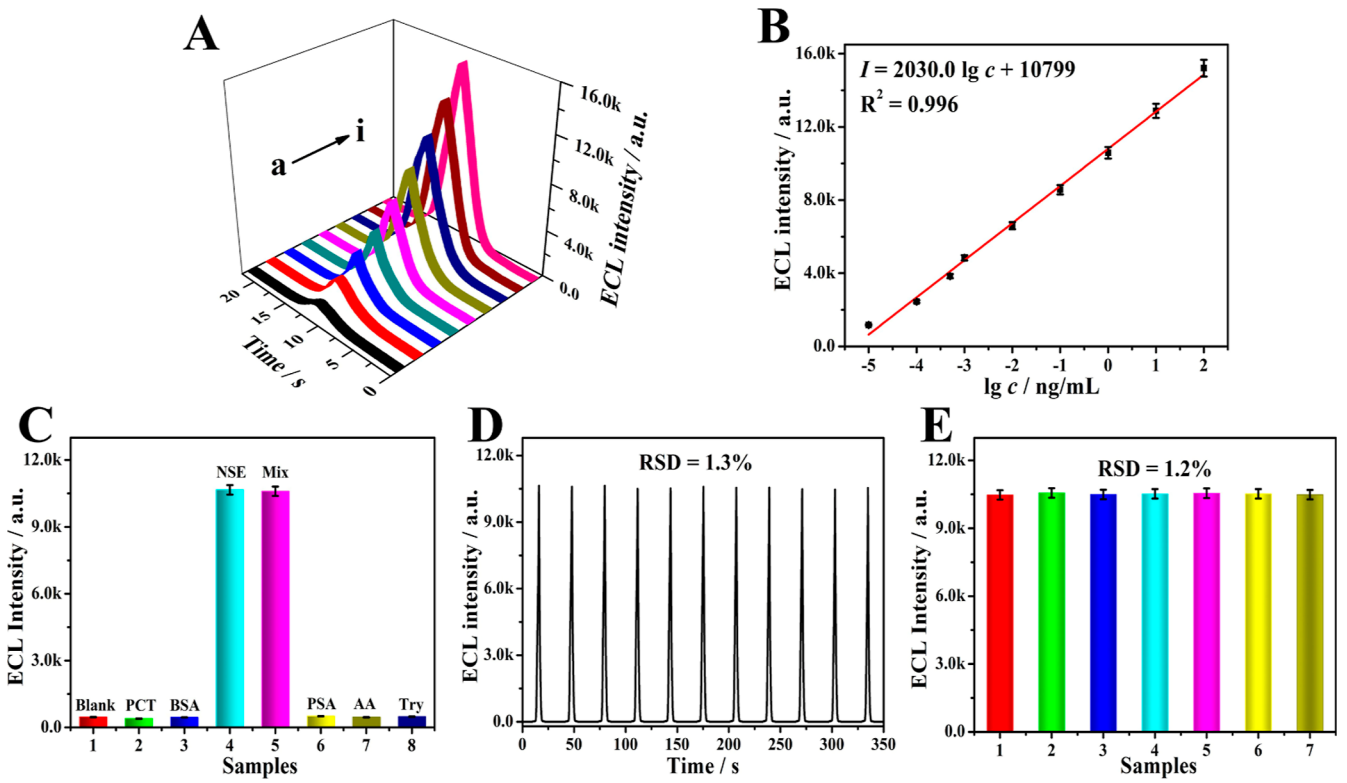

Figure 5. Performance tests of the proposed biosensor. (A) ECL responses of the biosensor at different concentrations of NSE (a–i: 0.00001, 0.0001, 0.0005, 0.001, 0.01, 0.1, 1, 10, and 100 ng/mL). (B) Calibration curve of the biosensor. (C) Selectivity, (D) stability, and (E) reproducibility of the biosensor.

Route 3:

$$O_2 + 2H_2O + 2e^- \rightarrow H_2O_2 + 2OH^- \quad (4)$$

$$Co^{2+}/Cu^{+} + H_2O_2 \rightarrow Co^{3+}/Cu^{2+} + OH^- + OH^{\bullet} \quad (5)$$

$$OH^{\bullet} + S_2O_8^{2-} \rightarrow O_2 + HSO_4^- + SO_4^{\bullet -}(\text{more}) \quad (6)$$

ECL emission:

$$PTCA + e^- \rightarrow PTCA^{\bullet -} \quad (7)$$

$$PTCA^{\bullet -} + SO_4^{\bullet -} \rightarrow PTCA^{*} + SO_4^{2-} \quad (8)$$

$$PTCA^{*} \rightarrow PTCA + h\nu \quad (9)$$

Calibration Curve for NSE Detection. In this work, the ECL signals of a range of different NSE concentrations were tested under optimal experimental conditions to study the detection ability of the biosensor (the conditional optimization process is shown in the Supporting Information). In Figure 5A, the ECL signals continued to rise with the increase in NSE concentrations. Figure 5B exhibits the linear correlation between ECL intensity and NSE concentrations (logarithm). The linear equation was I = 2030.0 lg c + 10799 (I: ECL intensity and c: NSE concentrations). Therefore, the proposed biosensor had a detection effect in the concentration range of 10 fg/mL to 100 ng/mL, and the calculated detection limit was 3.42 fg/mL (S/N = 3). Compared with other detection platforms (Table S1), this study realized more efficient NSE detection.

Performances of the Biosensor. To explore the performances of the developed biosensor, its selectivity was first tested. In Figure 5C, the ECL signals of the selected interferents (procalcitonin, BSA, prostate-specific antigen, ascorbic acid, and trypsin) were the same as those of the blank sample, which were far lower than the target detection signal. Meanwhile, the ECL signal of NSE was consistent with that of the mixed sample (1 ng/mL NSE + 10 ng/mL interferents), which confirmed that the biosensor had good selectivity. After that, we investigated the stability of the sensor according to the ECL responses measured by several cycles of continuous electrode scanning. In Figure 5D, the ECL signals had slight fluctuation with a relative standard deviation (RSD) of 1.3%. Finally, the reproducibility of the developed sensor was investigated according to the signals of seven different modified electrodes (Figure 5E). The results showed that the difference in the ECL signals measured using each electrode was very small (RSD = 1.2%), which verified the good reproducibility of the biosensor.

Analysis of Serum Samples. To evaluate practical the application ability of the biosensor, three different concentrations of human serum samples were selected to calculate RSD and recovery by standard addition method. As shown in Table S2, the obtained RSD and recovery were 1.5 to 2.3 and 97.5 to 103%, respectively, which indicated that the developed biosensor had excellent precision and accuracy in serum sample detection, showing great potential for clinical application.

CONCLUSIONS

In summary, a ternary ECL system using PTCA as a luminophore and Co_3O_4/CuO as a co-reaction promoter was designed for efficient NSE detection. First, the reduction of $S_2O_8^{2-}$ was greatly promoted due to the unique surface structure of Co_3O_4/CuO and the reversible conversion of Co^{3+}/Co^{2+} and Cu^{2+}/Cu^{+}, thus generating more $SO_4^{\bullet -}$ to

https://doi.org/10.1021/acssensors.2c00819
ACS Sens. 2022, 7, 2273−2280

amplify the ECL signal. Furthermore, NKF was used as a targeted antibody linker to enhance antibody incubation efficiency and maintain the activity of the biosensor. Hence, the detection sensitivity of the proposed biosensor was greatly improved. Finally, we combined a chip with ECL sensing analysis to improve the applicability of the sensor for practical applications. The developed biosensor chip had good stability and sensitivity, showing good application prospect in clinical real-time diagnosis.

■ ASSOCIATED CONTENT

Supporting Information

The Supporting Information is available free of charge at https://pubs.acs.org/doi/10.1021/acssensors.2c00819.

Chip preparation diagram, XPS spectra of Co_3O_4/CuO, electrochemical characterization of the proposed biosensor, optimization of experimental conditions, comparison with other detection platforms, and serum samples analysis (PDF)

■ AUTHOR INFORMATION

Corresponding Author

Yuyang Li − *Collaborative Innovation Center for Green Chemical Manufacturing and Accurate Detection, Key Laboratory of Interfacial Reaction & Sensing Analysis in Universities of Shandong, School of Chemistry and Chemical Engineering, University of Jinan, Jinan 250022 Shandong, China;* orcid.org/0000-0002-1399-9381; Phone: +86 531 82765730; Email: chm_liyy@ujn.edu.cn; Fax: +86 531 82765969

Authors

Xianzhen Song − *Collaborative Innovation Center for Green Chemical Manufacturing and Accurate Detection, Key Laboratory of Interfacial Reaction & Sensing Analysis in Universities of Shandong, School of Chemistry and Chemical Engineering, University of Jinan, Jinan 250022 Shandong, China*

Lu Zhao − *Collaborative Innovation Center for Green Chemical Manufacturing and Accurate Detection, Key Laboratory of Interfacial Reaction & Sensing Analysis in Universities of Shandong, School of Chemistry and Chemical Engineering, University of Jinan, Jinan 250022 Shandong, China*

Xiang Ren − *Collaborative Innovation Center for Green Chemical Manufacturing and Accurate Detection, Key Laboratory of Interfacial Reaction & Sensing Analysis in Universities of Shandong, School of Chemistry and Chemical Engineering, University of Jinan, Jinan 250022 Shandong, China*

Tao Feng − *Collaborative Innovation Center for Green Chemical Manufacturing and Accurate Detection, Key Laboratory of Interfacial Reaction & Sensing Analysis in Universities of Shandong, School of Chemistry and Chemical Engineering, University of Jinan, Jinan 250022 Shandong, China*

Hongmin Ma − *Collaborative Innovation Center for Green Chemical Manufacturing and Accurate Detection, Key Laboratory of Interfacial Reaction & Sensing Analysis in Universities of Shandong, School of Chemistry and Chemical Engineering, University of Jinan, Jinan 250022 Shandong, China;* orcid.org/0000-0002-7061-8944

Dan Wu − *Collaborative Innovation Center for Green Chemical Manufacturing and Accurate Detection, Key Laboratory of Interfacial Reaction & Sensing Analysis in Universities of Shandong, School of Chemistry and Chemical Engineering, University of Jinan, Jinan 250022 Shandong, China;* orcid.org/0000-0002-8732-5988

Chuannan Luo − *Collaborative Innovation Center for Green Chemical Manufacturing and Accurate Detection, Key Laboratory of Interfacial Reaction & Sensing Analysis in Universities of Shandong, School of Chemistry and Chemical Engineering, University of Jinan, Jinan 250022 Shandong, China*

Qin Wei − *Collaborative Innovation Center for Green Chemical Manufacturing and Accurate Detection, Key Laboratory of Interfacial Reaction & Sensing Analysis in Universities of Shandong, School of Chemistry and Chemical Engineering, University of Jinan, Jinan 250022 Shandong, China;* orcid.org/0000-0002-3034-8046

Complete contact information is available at: https://pubs.acs.org/10.1021/acssensors.2c00819

Notes

The authors declare no competing financial interest.

■ ACKNOWLEDGMENTS

This study was supported by the National Natural Science Foundation of China (no. 21777056 and no. 21427808), the Special Foundation for Taishan Scholar Professorship of Shandong Province (no. ts20130937), and the Jinan Scientific Research Leader Workshop Project (no. 2018GXRC024 and no. 2018GXRC021).

■ REFERENCES

(1) Liu, Z. Y.; Qi, W. J.; Xu, G. B. Recent advances in electrochemiluminescence. *Chem. Soc. Rev.* **2015**, *44*, 3117−3142.

(2) Ma, C.; Cao, Y.; Gou, X. D.; Zhu, J. J. Recent Progress in Electrochemiluminescence Sensing and Imaging. *Anal. Chem.* **2020**, *92*, 431−454.

(3) Khonsari, Y. N.; Sun, S. Recent trends in electrochemiluminescence aptasensors and their applications. *Chem. Commun.* **2017**, *53*, 9042−9054.

(4) Zhao, L.; Song, X. Z.; Ren, X.; Wang, H.; Fan, D. W.; Wu, D.; Wei, Q. Ultrasensitive near-infrared electrochemiluminescence biosensor derived from Eu-MOF with antenna effect and high efficiency catalysis of specific CoS2 hollow triple shelled nanoboxes for procalcitonin. *Biosens. Bioelectron.* **2021**, *191*, 113409.

(5) Zhou, Y.; Zheng, Y. Z.; Zhu, X. C.; Chai, Y. Q.; Yuan, R. Modular engineering of gold-silver nanocluster supermolecular structure endow strong electrochemiluminescence for ultrasensitive bioanalysis. *Biosens. Bioelectron.* **2021**, *190*, 113449.

(6) Zhao, L.; Song, X. Z.; Ren, X.; Fan, D. W.; Wei, Q.; Wu, D. Rare Self-Luminous Mixed-Valence Eu-MOF with a Self-Enhanced Characteristic as a Near-Infrared Fluorescent ECL Probe for Nondestructive Immunodetection. *Anal. Chem.* **2021**, *93*, 8613−8621.

(7) Zhao, L.; Wang, M.; Song, X. Z.; Liu, X. J.; Ju, H. X.; Ai, H.; Wei, Q.; Wu, D. Annihilation luminescent Eu-MOF as a near-infrared electrochemiluminescence probe for trace detection of trenbolone. *Chem. Eng. J.* **2022**, *434*, 134691.

(8) Chen, H.; Zhang, H.; Yuan, R.; Chen, S. Novel Double-Potential Electrochemiluminescence Ratiometric Strategy in Enzyme-Based Inhibition Biosensing for Sensitive Detection of Organophosphorus Pesticides. *Anal. Chem.* **2017**, *89*, 2823−2829.

(9) Li, S. J.; Liu, Y.; Ma, Q. Nanoparticle-based electrochemiluminescence cytosensors for single cell level detection. *TrAC, Trends Anal. Chem.* **2019**, *110*, 277−292.

(10) Chen, M. M.; Xu, C. H.; Zhao, W.; Chen, H. Y.; Xu, J. J. Single Cell Imaging of Electrochemiluminescence-Driven Photodynamic Therapy. *Angew. Chem., Int. Ed.* **2022**, *61*, 202117401.
(11) Ramirez-Celis, A.; Edmiston, E.; Schauer, J.; Vu, T.; Van de Water, J. Peptides of neuron specific enolase as potential ASD biomarkers: From discovery to epitope mapping. *Brain, Behav., Immun.* **2020**, *84*, 200−208.
(12) Haque, A.; Ray, S. K.; Cox, A.; Banik, N. L. Neuron specific enolase: a promising therapeutic target in acute spinal cord injury. *Metab. Brain Dis.* **2016**, *31*, 487−495.
(13) Ferraro, S.; Braga, F.; Luksch, R.; Terenziani, M.; Caruso, S.; Panteghini, M. Measurement of Serum Neuron-Specific Enolase in Neuroblastoma: Is There a Clinical Role? *Clin. Chem.* **2020**, *66*, 667−675.
(14) Hesari, M.; Workentin, M. S.; Ding, Z. F. NIR electrochemiluminescence from Au25− nanoclusters facilitated by highly oxidizing and reducing co-reactant radicals. *Chem. Sci.* **2014**, *5*, 3814−3822.
(15) Xu, C. M.; Luo, Y. L.; Li, S.; Li, Z. X.; Jiang, L.; Zhang, G. X.; Owusu, L.; Chen, H. L. Multifunctional neuron-specific enolase: its role in lung diseases. *Biosci. Rep.* **2019**, *39*, 20192732.
(16) Song, X. Z.; Shao, X. R.; Dai, L.; Fan, D. W.; Ren, X.; Sun, X.; Luo, C. N.; Wei, Q. Triple Amplification of 3,4,9,10-Perylenetetracarboxylic Acid by Co2+-Based Metal-Organic Frameworks and Silver-Cysteine and Its Potential Application for Ultrasensitive Assay of Procalcitonin. *ACS Appl. Mater. Interfaces* **2020**, *12*, 9098−9106.
(17) Lei, Y. M.; Wen, R. X.; Zhou, J.; Chai, Y. Q.; Yuan, R.; Zhuo, Y. Silver Ions as Novel Coreaction Accelerator for Remarkably Enhanced Electrochemiluminescence in a PTCA-S2O82- System and Its Application in an Ultrasensitive Assay for Mercury Ions. *Anal. Chem.* **2018**, *90*, 6851−6858.
(18) Liu, Y.; Wang, H.; Xiong, C.; Chai, Y.; Yuan, R. An ultrasensitive electrochemiluminescence immunosensor for NT-proBNP based on self-catalyzed luminescence emitter coupled with PdCu@carbon nanohorn hybrid. *Biosens. Bioelectron.* **2017**, *87*, 779−785.
(19) Zhang, H.; Zuo, F.; Tan, X.; Xu, S.; Yuan, R.; Chen, S. A novel electrochemiluminescent biosensor based on resonance energy transfer between poly(9,9-di- n -octylfluorenyl-2,7-diyl) and 3,4,9,10-perylenetetracar-boxylic acid for insulin detection. *Biosens. Bioelectron.* **2018**, *104*, 65−71.
(20) Zhang, P.; Zhuo, Y.; Chang, Y.; Yuan, R.; Chai, Y. Electrochemiluminescent Graphene Quantum Dots as a Sensing Platform: A Dual Amplification for MicroRNA Assay. *Anal. Chem.* **2015**, *87*, 10385−10391.
(21) Zhang, Y.; Huang, J.; Ding, Y. Porous Co 3 O 4 /CuO hollow polyhedral nanocages derived from metal-organic frameworks with heterojunctions as efficient photocatalytic water oxidation catalysts. *Appl. Catal., B* **2016**, *198*, 447−456.
(22) Makaraviciute, A.; Ramanaviciene, A. Site-directed antibody immobilization techniques for immunosensors. *Biosens. Bioelectron.* **2013**, *50*, 460−471.
(23) Dostalova, S.; Cerna, T.; Hynek, D.; Koudelkova, Z.; Vaculovic, T.; Kopel, P.; Hrabeta, J.; Heger, Z.; Vaculovicova, M.; Eckschlager, T.; Stiborova, M.; Adam, V. Site-Directed Conjugation of Antibodies to Apoferritin Nanocarrier for Targeted Drug Delivery to Prostate Cancer Cells. *ACS Appl. Mater. Interfaces* **2016**, *8*, 14430−14441.
(24) Liu, F.; Wang, L.; Wang, H. W.; Yuan, L.; Li, J. W.; Brash, J. L.; Chen, H. Modulating the Activity of Protein Conjugated to Gold Nanoparticles by Site-Directed Orientation and Surface Density of Bound Protein. *ACS Appl. Mater. Interfaces* **2015**, *7*, 3717−3724.
(25) Sugita, T.; Katayama, M.; Okochi, M.; Kato, R.; Ichihara, T.; Honda, H. Screening of peptide ligands that bind to the Fc region of IgG using peptide array and its application to affinity purification of antibody. *Biochem. Eng. J.* **2013**, *79*, 33−40.
(26) Jia, Y.; Yang, L.; Xue, J. W.; Zhang, N.; Fan, D. W.; Ma, H. M.; Ren, X.; Hu, L. H.; Wei, Q. Bioactivity-Protected Electrochemiluminescence Biosensor Using Gold Nanoclusters as the Low-Potential Luminophor and Cu2S Snowflake as Co-reaction Accelerator for Procalcitonin Analysis. *ACS Sens.* **2019**, *4*, 1909−1916.
(27) Wang, C.; Han, Q.; Liu, P. K.; Zhang, G.; Song, L.; Zou, X. C.; Fu, Y. Z. A Superstable Luminescent Lanthanide Metal Organic Gel Utilized in an Electrochemiluminescence Sensor for Epinephrine Detection with a Narrow Potential Sweep Range. *ACS Sens.* **2021**, *6*, 252−258.
(28) Bahari, D.; Babamiri, B.; Moradi, K.; Salimi, A.; Hallaj, R. Graphdiyne nanosheet as a novel sensing platform for self-enhanced electrochemiluminescence of MOF enriched ruthenium (II) in the presence of dual co-reactants for detection of tumor marker. *Biosens. Bioelectron.* **2022**, *195*, 113657.
(29) Li, F.; Yang, H.; Shan, C.; Zhang, Q.; Han, D.; Ivaska, A.; Niu, L. The synthesis of perylene-coated graphene sheets decorated with Au nanoparticles and its electrocatalysis toward oxygen reduction. *J. Mater. Chem.* **2009**, *19*, 4022−4025.
(30) Fu, X.; Yang, Y.; Wang, N.; Chen, S. The electrochemiluminescence resonance energy transfer between Fe-MIL-88 metal-organic framework and 3,4,9,10-perylenetetracar-boxylic acid for dopamine sensing. *Sens. Actuators, B* **2017**, *250*, 584−590.
(31) Menezes, P. W.; Indra, A.; González-Flores, D.; Sahraie, N. R.; Zaharieva, I.; Schwarze, M.; Strasser, P.; Dau, H.; Driess, M. High-Performance Oxygen Redox Catalysis with Multifunctional Cobalt Oxide Nanochains: Morphology-Dependent Activity. *ACS Catal.* **2015**, *5*, 2017−2027.
(32) Wei, J.; Feng, Y.; Liu, Y.; Ding, Y. MxCo3−xO4 (M = Co, Mn, Fe) porous nanocages derived from metal-organic frameworks as efficient water oxidation catalysts. *J. Mater. Chem. A* **2015**, *3*, 22300−22310.
(33) Li, J.; Wang, J.; Liang, X.; Zhang, Z.; Liu, H.; Qian, Y.; Xiong, S. Hollow MnCo2O4 Submicrospheres with Multilevel Interiors: From Mesoporous Spheres to Yolk-in-Double-Shell Structures. *ACS Appl. Mater. Interfaces* **2014**, *6*, 24−30.
(34) Kumar, D. R.; Manoj, D.; Santhanalakshmi, J.; Shim, J. J. Au-CuO core-shell nanoparticles design and development for the selective determination of Vitamin B6. *Electrochim. Acta* **2015**, *176*, 514−522.
(35) Chen, M.; Hou, C.; Huo, D.; Yang, M.; Fa, H. An ultrasensitive electrochemical DNA biosensor based on a copper oxide nanowires/single-walled carbon nanotubes nanocomposite. *Appl. Surf. Sci.* **2016**, *364*, 703−709.
(36) Jiao, F.; Frei, H. Nanostructured cobalt oxide clusters in mesoporous silica as efficient oxygen-evolving catalysts. *Angew. Chem., Int. Ed.* **2009**, *48*, 1841−1844.
(37) Rosen, J.; Hutchings, G. S.; Jiao, F. Ordered Mesoporous Cobalt Oxide as Highly Efficient Oxygen Evolution Catalyst. *J. Am. Chem. Soc.* **2013**, *135*, 4516−4521.
(38) Wang, Z. J.; Sun, P. Z.; Li, Y. X.; Meng, T.; Li, Z. P.; Zhang, X.; Zhang, R. C.; Jia, H. Z.; Yao, H. Reactive Nitrogen Species Mediated Degradation of Estrogenic Disrupting Chemicals by Biochar/Monochloramine in Buffered Water and Synthetic Hydrolyzed Urine. *Environ. Sci. Technol.* **2019**, *53*, 12688−12696.
(39) Liu, J. L.; Yang, R.; Chai, Y. Q.; Yuan, R. Versatile Luminol/Dissolved Oxygen/Fe@Fe2O3 Nanowire Ternary Electrochemiluminescence System Combined with Highly Efficient Strand Displacement Amplification for Ultrasensitive microRNA Detection. *Anal. Chem.* **2021**, *93*, 13334−13341.
(40) Wang, Y.; Liu, L. H.; Fang, G. D.; Wang, L.; Kengara, F. O.; Zhu, C. Y. The mechanism of 2-chlorobiphenyl oxidative degradation by nanoscale zero-valent iron in the presence of dissolved oxygen. *Environ. Sci. Pollut. Res.* **2018**, *25*, 2265−2272.
(41) Fang, G. D.; Liu, C.; Gao, J.; Dionysiou, D. D.; Zhou, D. M. Manipulation of Persistent Free Radicals in Biochar To Activate Persulfate for Contaminant Degradation. *Environ. Sci. Technol.* **2015**, *49*, 5645−5653.

https://doi.org/10.1021/acssensors.2c00819
ACS Sens. 2022, 7, 2273−2280